Journal of the Ceramic Society of Japan 125 [4] 262-267 2017 Full paper

Li-rich layered cathode microparticle $0.4Li_2MnO_3 \cdot 0.6Li(Mn_{0.43}Ni_{0.36}Co_{0.21})O_2$ decorated with nanosized grains

Jung Yoon SEO[*,], Sung Nam LIM[***], Seung Bin PARK[*] and Dae Soo JUNG[****,†]**

[*]Department of Chemical and Biomolecular Engineering, Korea Advanced Institute of Science and Technology, 291 Daehak-ro, Yuseong-gu, Daejeon 34141, Republic of Korea
[**]Global Nanotechnology Development Team, National NanoFab Center (NNFC), 291 Daehak-ro, Yuseong-gu, Daejeon 34141, Republic of Korea
[***]Micro/Nano Scale manufacturing group, Korea Institute of Industrial Technology, 143 Hanggaulro, Sangrok-gu, Ansan-si, Gyeonggi-do 15588, Republic of Korea
[****]Energy & Environmental Division, Korea Institute of Ceramic Engineering & Technology (KICET), 101 Soho-ro, Jinju-si, Gyeongsangnam-do 52851, Republic of Korea

A lithium-rich layered cathode material [$0.4Li_2MnO_3 \cdot 0.6Li(Mn_{0.43}Ni_{0.36}Co_{0.21})O_2$)] containing nanosized grains (50–100 nm) was prepared from an aqueous precursor solution via a sequential two-step process composed of ultrasonic spray pyrolysis and post-calcination. The microsized lithium-rich layered composites show a high initial discharge capacity of 251 mA h g^{-1} at 0.1 C. The reversible capacities of 206 mA h g^{-1} at 0.5 C and 189 mA h g^{-1} at 1 C are obtained between 4.6 and 2.0 V. These are comparable to the values reported previously for these materials, without the need for doping or surface modification. The improved electrochemical performance may have resulted from the presence of nanosized grains, which can lead to an improvement in electronic and ionic transport, and the homogeneously dispersed Li_2MnO_3 phase in the $LiMO_2$ (M = Mn, Ni, Co) phase. These results suggest that spray pyrolysis is an effective technique for the preparation of multi-component composite materials and can be used to control the microstructure of the materials, ultimately improving the electrical performance.

Key-words : Layered oxide cathode, Electrochemical performance, Energy efficiency, Spray pyrolysis, Lithium-ion battery

[Received October 6, 2016; Accepted December 12, 2016]

1. Introduction

Coping with climate change has become one of the most important issues of this era. In this regard, many researchers in various fields have worked on the sequestration of greenhouse gases.[1] Transportation sector accounts for almost 14% of global greenhouse gas emissions. Therefore, replacing fossil fuel-based vehicles with electric vehicles is a key strategy to reducing greenhouse gas emissions. This need promotes the development of high-capacity energy storage systems.[2]

Among the various types of batteries, lithium-ion batteries are considered the most attractive option because of their light weight and high power density.[3)–5)] However, current performance is not satisfactory for the full-scale commercialization of electric vehicles (EVs) and hybrid electric vehicles (HEVs).[6] Increasing the driving range and reducing battery costs remain key issues that need to be addressed.

Li-rich layered cathode materials [$xLi_2MnO_3 \cdot (1-x)$ $LiMO_2$ (M = Ni, Co, Mn)] are gaining popularity because of their high capacities, broad voltage range (~4.6 V), low cost, and high stability[7)–11)] compared to commercial $LiCoO_2$.[12),13)] However, layered $xLi_2MnO_3 \cdot (1-x)LiMO_2$ shows a low-rate capability because of its low electronic conductivity, which is caused by the insulating $Li[Li_{1/3}Mn_{2/3}]O_2$ component.[14),15)] Therefore, the low-rate capabilities of these batteries need to be improved for their use in EVs and HEVs, which require fast charge/discharge reactions.

Various methods have been developed to enhance the rate capability of Li-rich layered cathode materials such as heteroatom doping, surface modification, and coating.[14),16),17)] However, attempts to control the morphology and particle size have rarely been accomplished because of limitations of preparation methods. The cathode materials are normally prepared by solid-state reactions or liquid-phase methods requiring a high calcination temperature and long calcination time to obtain the desired composite phase.[18)–20)] These calcination conditions result in the aggregation and growth of primary particles, which disrupt the diffusion of Li-ions between the electrode and the electrolyte.

In recent studies, spray pyrolysis has attracted attention for the fabrication of multicomponent ceramic particles owing to its prominent advantages of simplicity, controllability, and capability to produce particles with high crystallinity[21)–24)] In this study, we prepared spherical $0.4Li_2MnO_3 \cdot 0.6Li(Mn_{0.43}Ni_{0.36}Co_{0.21})O_2$ microparticles containing nanosized grains by spray pyrolysis and a post-heat treatment. Additionally, the structural and electrochemical properties of the prepared microparticles were investigated.

2. Experimental procedure

2.1 Preparation of Li-rich layered cathode microparticles

Spray pyrolysis process was used to produce Li-rich layered oxide microparticles of the cathode material, $0.4Li_2MnO_3 \cdot 0.6Li(Mn_{0.43}Ni_{0.36}Co_{0.21})O_2$. The detailed description of this

† Corresponding author: D. S. Jung; E-mail: dsjung@kicet.re.kr
‡ Preface for this article: DOI http://doi.org/10.2109/jcersj2.125.P4-1

DOI http://doi.org/10.2109/jcersj2.16217

process was presented in our previous report.[25] The reaction temperature and flow rate of the carrier gas (air) were fixed at 800°C and 15 L min^{-1}, allowing the residence time of precursor droplets in the reactor to be 1.6 s. The concentration of the aqueous precursor solution was adjusted to 0.5 mol L^{-1} of the title compound with suitable quantities of lithium nitrate ($LiNO_3$, 98%, Junsei), manganese nitrate [$Mn(NO_3)_2{\cdot}6H_2O$, 98%, Kanto], nickel nitrate [$Ni(NO_3)_2{\cdot}6H_2O$, 98%, Junsei], and cobalt nitrate [$Co(NO_3)_2{\cdot}6H_2O$, 97%, Junsei]. The microparticles prepared by this process were calcined at temperatures between 600 and 1000°C for 12 h to understand the effect of calcination on cycle stability and rate capability.

2.2 Characterization of Li-rich layered cathode microparticles

The crystal structures of the $0.4Li_2MnO_3{\cdot}0.6Li(Mn_{0.43}Ni_{0.36}Co_{0.21})O_2$ microparticles were confirmed by X-ray diffractometry [XRD; Rigaku, D/MAX-2500 (18 kW)] with filtered Cu K_α radiation. The Brunauer–Emmett–Teller technique (BET; Micrometrics, ASAP2010) was employed to measure the total surface area of the microparticles. The size distribution was obtained using a particle size analyzer (Cilas, 1064). The morphological properties were analyzed by field-emission scanning electron microscopy (FE-SEM; HITACHI, S-4800) and field-emission transmission electron microscopy (FE-TEM; FEI, Tecnai G2 F30). The thermal properties of the microparticles were determined by thermogravimetry-differential scanning calorimetry (TG-DSC; Setaram, Setsys 16/18).

The slurry for preparing the electrode was composed of the active material (88 wt %), polyvinylidene difluoride (5.5 wt %), and carbon black (Denka, 6.5 wt %). The slurry was cast on aluminum foil and dried at 130°C for 30 min. The electrode was pressed with a rolling machine to obtain a material with a porosity of 33% and then punched into 15-mm-diameter disks. Lithium foil (Hohsen Corporation) was used as the negative electrode and the electrolyte solution was 1 M $LiPF_6$ in solvent. All procedures used to prepare the cell were performed in a dry room. The assembled cells were aged for 24 h before the first charge to ensure full absorption of the electrolyte into the electrode. Electrochemical performances were evaluated between 4.6 and 2.0 V at 25°C using a TOSCAT 3100 series electrochemical bench. For rate capability, various current rates (0.1, 0.2, 0.5, 1, and 2 C; where 1 C = 200 mA h g^{-1}) were applied. After rate capability measurements, the cycle stability was evaluated at a rate of 0.5 C.

3. Results and discussion

The microparticles prepared by spray pyrolysis have a spherical morphology with a mean diameter of 1.59 μm (**Fig. 1**). The TG-DSC curves of the microparticles show three weight-loss regions (**Fig. 2**). The first weight-loss region observed at a temperature below 150°C is related to the evaporation of water molecules adsorbed on the precursor particles. The second weight-loss step (150–600°C) is attributed to the decomposition of nitrate precursors and the formation of the $LiMO_2$ (M = Ni, Co, Mn) phase. The last step is speculated to be the formation of the Li_2MnO_3 phase, which will be explained later in the paper using XRD results (**Fig. 5**). The total weight loss was about 10 wt %. The slight weight loss around 1000°C can be attributed to the evaporation of Li.[26] According to the TG-DSC analysis, it can be clearly seen that post-heat treatment is required for the formation of the composite structures. Here, it was supposed that post-heat treatment did not cause large variation in chemical compositions except 1000°C where the volatilization of lithium could severely

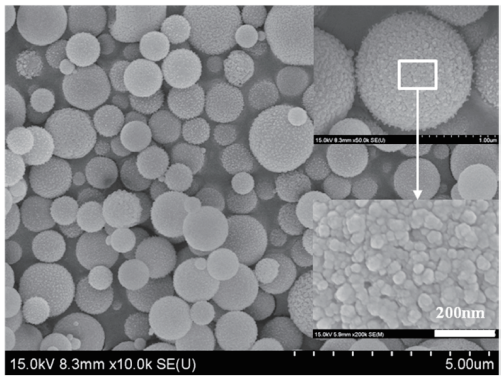

(a)

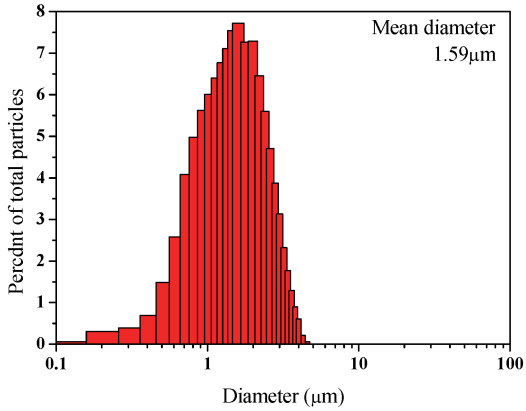

(b)

Fig. 1. (a) SEM images and (b) particle size distribution of as-prepared $0.4Li_2MnO_3{\cdot}0.6Li(Mn_{0.43}Ni_{0.36}Co_{0.21})O_2$ microparticles via spray pyrolysis process.

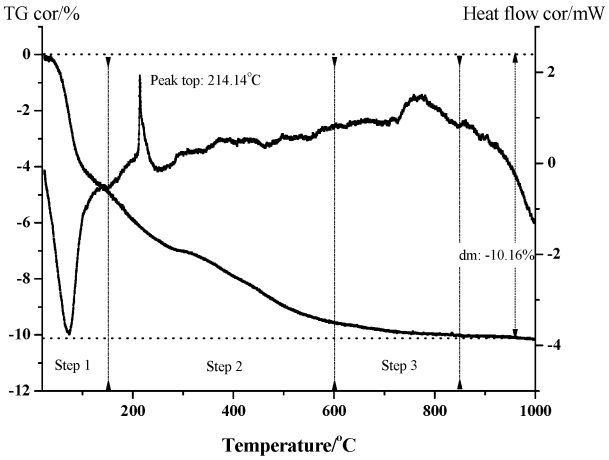

Fig. 2. TG/DSC curves of as-prepared $0.4Li_2MnO_3{\cdot}0.6Li(Mn_{0.43}Ni_{0.36}Co_{0.21})O_2$ microparticles.

occur. Because, the post-heat treatment condition in this study is very mild compared to those in literatures, leading to significant loss of lithium content.[26]

The SEM and TEM images of the $0.4Li_2MnO_3{\cdot}0.6Li(Mn_{0.43}Ni_{0.36}Co_{0.21})O_2$ microparticles calcined at different temperatures are presented in **Fig. 3**. The microparticles calcined at 700°C were aggregate-free and had a morphology similar to that of the as-prepared microparticles. Grain growth of the primary particles—nanosized grains having diameters ranging from 10 to 50 nm—

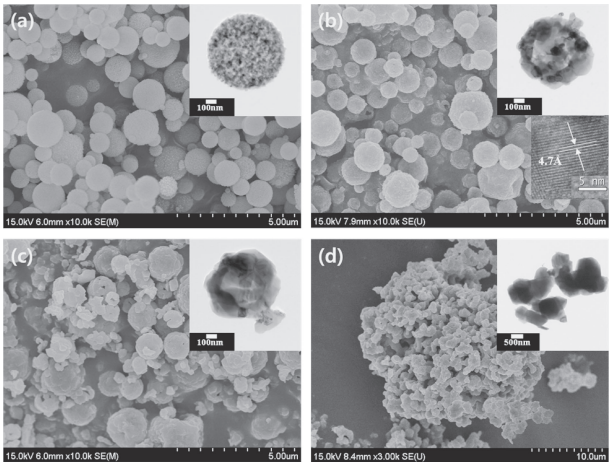

Fig. 3. SEM and TEM images of $0.4Li_2MnO_3 \cdot 0.6Li(Mn_{0.43}Ni_{0.36}Co_{0.21})O_2$ microparticles calcined at (a) 700, (b) 800, (c) 900, and (d) 1000°C.

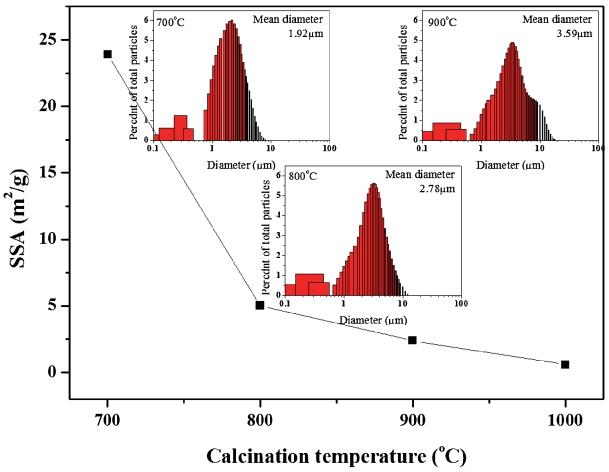

Fig. 4. Variation of the specific surface area and particle size distribution of $0.4Li_2MnO_3 \cdot 0.6Li(Mn_{0.43}Ni_{0.36}Co_{0.21})O_2$ microparticles calcined at different temperature.

was not observed in the sample calcined at 700°C. However, grain growth occurred at calcination temperatures of 800°C and higher, and the diameter of the primary particles increased to 50–100 nm. When the calcination temperature was increased up to 1000°C, the microparticles began to aggregate and had a diameter of 20–30 μm.

The average size of the primary particles increased from 30 to 600 nm as the calcination temperature was increased from 700 to 1000°C. The HRTEM image [Fig. 3(b)] shows an enlarged view of the microcomposites, where the lattice spacing of 0.47 nm signifies the (001) fringes of Li_2MnO_3 and (003) fringes of $LiMO_2$ (M = Ni, Co, Mn).[7] It is difficult to distinguish the formation of the Li_2MnO_3 and $LiMO_2$ phases by HRTEM because lattice fringes of both overlap. Thus, results of XRD analysis were used to demonstrate the formation of the Li_2MnO_3 and $LiMO_2$ phases.

Figure 4 shows the effect of calcination temperature on the particle size distribution (PSD) and specific surface area of $0.4Li_2MnO_3 \cdot 0.6Li(Mn_{0.43}Ni_{0.36}Co_{0.21})O_2$ microparticles. The surface area decreased from 23.9 to 0.59 $m^2 g^{-1}$ as the calcination temperature was increased from 700 to 1000°C; there was a dramatic drop in the surface area at the calcination temperature of 800°C. The mean particle size increased from 1.92 to 3.59 μm

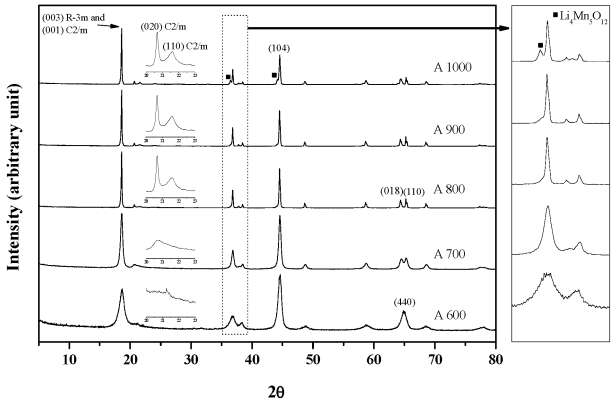

Fig. 5. XRD patterns of $0.4Li_2MnO_3 \cdot 0.6Li(Mn_{0.43}Ni_{0.36}Co_{0.21})O_2$ microparticles calcined at different temperature.

when the calcination temperature was increased from 700 to 900°C. The results of PSD analysis were consistent with the morphology characteristics shown in Fig. 3.

XRD patterns of the calcined $0.4Li_2MnO_3 \cdot 0.6Li(Mn_{0.43}Ni_{0.36}Co_{0.21})O_2$ microparticles are presented in Fig. 5. $LiMO_2$ (M = Ni, Co, Mn) in the microcomposites has a hexagonal α-$NaFeO_2$ structure with a space group of $R\bar{3}m$. The degree of ordering in the layered structure of the $LiMO_2$ can be assessed based on the formation of split peaks at 2θ 64–66° corresponding to the (018) and (110) reflections.[20] The splitting of the peak clearly occurred in the microparticles calcined at temperatures ≥800°C. The composite particles calcined at 700°C also contained split peaks, but the degree of splitting was not distinct. In the XRD pattern of the particles calcined at 600°C, split peaks were not observed.

The structure of Li_2MnO_3 is similar to that of the $LiMO_2$ with an $R\bar{3}m$ layered rock-salt structure.[27] However, Li_2MnO_3 has a monoclinic structure with a space group of C2/m formed by the super-lattice ordering of Li^+ and Mn^{4+}, which exists in the transition metal (TM) layer. Small satellite peaks located at 22° (2θ) are indicative of the formation of the Li_2MnO_3 phase.[7),28] In addition, the microparticles calcined at temperatures above 700°C exhibit diffraction peaks. However, the peaks of the microparticles calcined at 700°C appear to be highly disordered, given that some peaks are broadened. A disordered peak indicates a high density of stacking disorders, which can cause an increase in the capacity but a rapid decrease in cycle stability. Moreover, the microparticles calcined at 1000°C have secondary $Li_4Mn_5O_{12}$ peaks at 38 and 43°, which could be attributed to the evaporation of Li-ions.[29] Thus, these results indicate that microparticles with good electrochemical performance can be obtained when the particles are calcined between 800 and 900°C; low crystallinity and the formation of a secondary phase are not suitable for high performance cathode materials.[30]

Figure 6 shows the initial charge/discharge curves of the calcined $0.4Li_2MnO_3 \cdot 0.6Li(Mn_{0.43}Ni_{0.36}Co_{0.21})O_2$ microparticles in different temperatures cycled in the voltage range of 2.0–4.6 V at a current density of 0.1 C (where 1 C = 200 mA h g^{-1}). All the initial charge curves have two clearly distinguishable voltage regions. Region A of the curves, exhibiting a plateau at ~4.5 V, corresponds to the oxidation of nickel and cobalt at <4.5 V and region B corresponds to the irreversible loss of oxygen due to the decomposition reaction by the activation of Li_2MnO_3 at >4.5 V. Considering this result, the calcined microparticles at 700°C are desirable, of which temperature are relatively lower than those of other solid-state reaction or liquid-phase methods.[31] Lim et al.

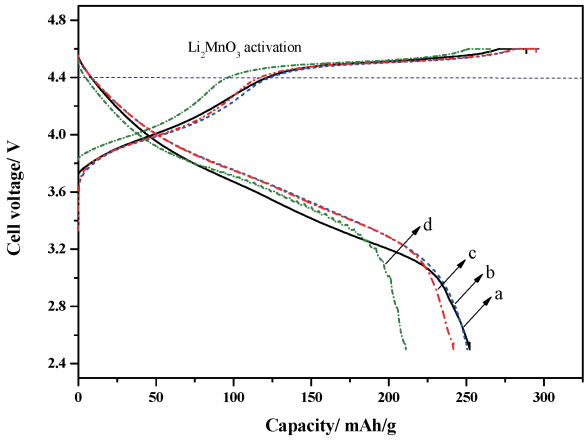

Sintering temp. (°C)	1st Charge	1st Discharge (mAh/g)	*CE (%)	$I_{020}Li_2MnO_3$ (C2/m): I_{003} $LiMn_{0.43}Ni_{0.36}Co_{0.21}O_2$ (R-3m)
700	289	251	87	
800	297	251	85	0.047751
900	296	242	82	0.050434
1000	266	211	80	0.053214

*CE: first-cycle coulombic efficiency

Fig. 6. 1st charge and discharge curves of $0.4Li_2MnO_3{\cdot}0.6Li(Mn_{0.43}Ni_{0.36}Co_{0.21})O_2$ microparticles calcined at (a) 700, (b) 800, (c) 900 and (d) 1000°C, cycled in the voltage range of 2.0–4.6 V at the current density of 0.1C.

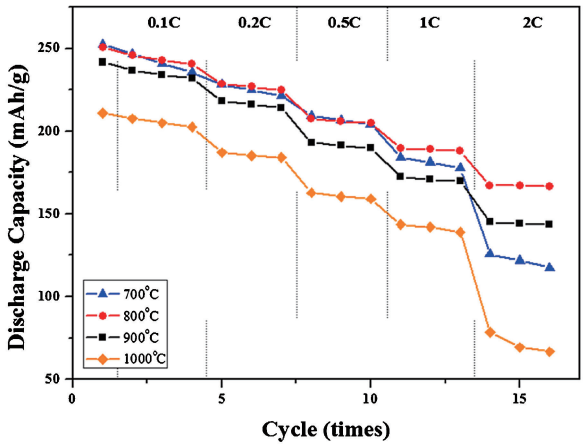

Sintering temp. (°C)	Discharge capacities at different C-rate, ($mAhg^{-1}$)					
	0.1C	0.2C	0.5C	1C	2C	1C/0.1C
700°C	241.0	224.9	206.7	180.9	121.6	0.75
800°C	243.1	226.8	205.9	188.8	166.9	0.78
900°C	234.2	216.2	191.4	170.9	144.3	0.73
1000°C	205.0	185.5	160.9	141.5	71.5	0.69

Fig. 7. Comparison of rate capability of $0.4Li_2MnO_3{\cdot}0.6Li(Mn_{0.43}Ni_{0.36}Co_{0.21})O_2$ microparticles calcined at different temperature, cycled in the voltage range of 2.0–4.6 V.

found that an increase in the Li_2MnO_3 content of the composites resulted in a shift to higher voltage in the initial charge curve and the voltage plateau (at 4.45 V) became longer.[19] Johnson et al. used the I_{020}/I_{003} intensity ratio ($C2/m/R\bar{3}m$) as a rough guide for determining the Li_2MnO_3 content in $xLiMnO_3{\cdot}(1-x)LiMO_2$ composite particles.[32] A shift in the initial charge curve was also observed for our $0.4Li_2MnO_3{\cdot}0.6Li(Mn_{0.43}Ni_{0.36}Co_{0.21})O_2$ microcomposites. In addition, an increase in the intensity ratio from 0.047 to 0.053 was observed as the calcination temperature was increased. Moreover, the first-cycle coulombic efficiency (CE) decreased from 87 to 80%, as the calcination temperature was increased, as shown in the inserted table in Fig. 6. These results indicate that the Li_2MnO_3 content in the $xLiMnO_3{\cdot}(1-x)LiMO_2$ increased. This is because the irreversible capacity loss on the initial charge and discharge results from electrochemical activation involving Li_2O extraction from Li_2MnO_3.[33] Thus, based on the aforementioned results, we can conclude that an increase in the calcination temperature increases the content of Li_2MnO_3 in $xLiMnO_3{\cdot}(1-x)LiMO_2$.

The initial discharge capacities of the calcined microparticles decreased with increasing calcination temperature: 251 mA h g^{-1} at 700 and 800°C, 242 mA h g^{-1} at 900°C, and 211 mA h g^{-1} at 1000°C. Although the initial charge and discharge capacities were reported to increase with an increase in the Li_2MnO_3 content,[19] in this study, the microparticles calcined at 700°C had a low Li_2MnO_3 content but a high initial discharge capacity of 251 mA h g^{-1}. This could be explained by the disordered peak containing a high density of stacking disorders, as shown in Fig. 5. Normally, a material without defects has the lowest energy state; defects in materials increase the energy state.[34] Thus, the composites with defects lowered the activation barrier for Li diffusion and enabled Li to be extracted at a lower potential, which increased the initial capacity.

Moreover, the capacity decreased with an increase in the calcination temperature, although the Li_2MnO_3 content increased. This was due to an increase in the particle size and a decrease in the surface area. When the particle size increases, lithium diffusion becomes difficult because of the barrier to diffusion for the Li-ions within a cathode particle and the difficulty in electron transport through the bulk of the cathode particle.[35] The capacity of the microparticles calcined at 1000°C largely decreases. This is thought to be due to the formation of $Li_4Mn_5O_{12}$ by evaporation of the Li-ions at a high calcination temperature (Fig. 5). Thus, in this study, the capacity did not appear to be strongly affected by the increase of Li_2MnO_3 content in $xLiMnO_3{\cdot}(1-x)LiMO_2$ microparticles, but rather by the morphology, specific surface area, and crystal structure. The microparticles calcined at 800°C were decorated with nanosized grains, and thus had the highest capacity (251 mA h g^{-1}).

To investigate the effect of calcination temperature on the rate capability of $0.4Li_2MnO_3{\cdot}0.6Li(Mn_{0.43}Ni_{0.36}Co_{0.21})O_2$, the calcined microparticles were galvanostatically charged at a current density of 0.1 C before each discharging test, and then the current density was changed from 0.1 to 2 C. **Figure 7** shows the rate capability of the microparticles cycled over a voltage range of 2.0–4.6 V. The specific surface areas of the microparticles decreased with increasing the calcination temperature (Fig. 4). The rate capability is related to the specific surface area and primary particle size of the microparticles. Increase in the surface area and decrease in primary particle size accelerate the diffusion of Li ions in the composite particles—due to their short diffusion pathway—which improves the rate capability. Thus, the spherical microparticles with nanosized grains and pure well-crystallized phase (calcined at 800°C) showed a good rate performance. However, the capacity of the microparticles calcined at 700°C showed a high initial discharge capacity; the capacity decreased sharply as the current density increased, which can be explained based on the XRD and BET analyses. The microparticles had high capacity due to the disordered peak and high surface area (mentioned above), did not have a well-ordered layered structure

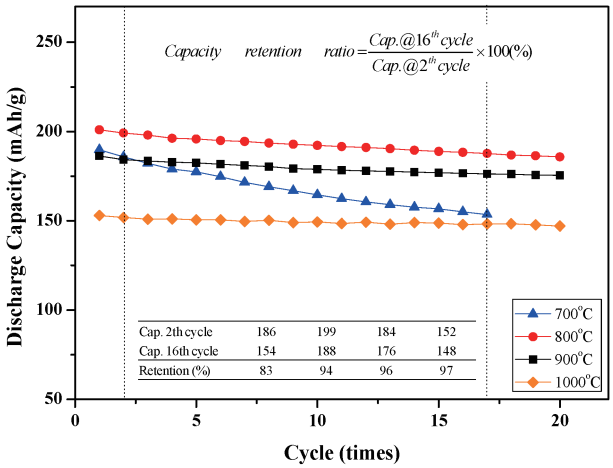

Fig. 8. Comparison of the capacity vs. cycle number of $0.4Li_2MnO_3 \cdot 0.6Li(Mn_{0.43}Ni_{0.36}Co_{0.21})O_2$ microparticles calcined at different temperature (in the voltage range of 2.0–4.6 V at the current density of 0.5C).

of $LiMO_2$, and had crystal defects in Li_2MnO_3. These factors can result in an unstable cycle property, especially for a high cut-off voltage and high current density. Moreover, the microparticles calcined at 1000°C showed a rapid decrease in capacity at the high current density of 2 C, which was attributed to the large grain size and low surface area ($0.59\,m^2\,g^{-1}$). To sum up, the rate capability was maximized with a sample calcined at 800°C although the sample calcined at 800°C had lower surface area than that of the samples at 700°C. It was because the sample had not only optimal point in primary grain size and specific surface, but also well-developed crystal structures.

Figure 8 shows the capacity retention of $0.4Li_2MnO_3 \cdot 0.6Li(Mn_{0.43}Ni_{0.36}Co_{0.21})O_2$ microparticles over the voltage range of 2.0–4.6 V at 25°C and a current density of 0.5 C. Testing was done after the rate capability test. Thus, the capacity retention ratio was calculated using the equation shown in Fig. 8. All the composite particles showed a stable charge/discharge capacity after 16 cycles at 25°C, except the microparticles calcined at 700°C. The microparticles calcined at 700°C retained 83% of their initial capacity after 16 cycles, which resulted from the unstable structure and high surface area, as shown in Figs. 3 and 4. The high surface area of cathode materials could, to some degree, help in improving the rate capability, but has negative side effects such as side reactions with electrolyte or dissolutions of transition metal, which finally degrade cycle performance.[33),36),37)]

Conversely, the microparticles calcined at 800 and 900°C delivered a reasonably steady capacity and retention ratio, as shown in the table inserted in Fig. 8. This occurred because the primary particle size was large enough to minimize side-reactions with the electrolyte, the formation of Li_2MnO_3 (which served as a stabilizer), and the well-developed layered structure of $LiMO_2$. The slight difference in capacity could be attributed to the difference in surface area. The microparticles calcined at 1000°C had excellent cycling performance (97% after 16 cycles), but considerably lower capacity due to the increase in the diffusion pathway caused by the large particle size and secondary phase.

4. Conclusions

Spherical $0.4Li_2MnO_3 \cdot 0.6Li(Mn_{0.43}Ni_{0.36}Co_{0.21})O_2$ microparticles with nanosized grains were successfully prepared by a two-step process: spray pyrolysis followed by low-temperature calcination. The microstructure and crystal structure were strongly dependent on the calcination temperature, which affected the electrochemical performance. The good rate capability and cycle stability of the microparticles calcined at 800°C were ascribed to the following factors: (1) the formation of a well-developed Li_2MnO_3 phase, which supplies surplus Li-ions to the $LiMO_2$ component as a stabilizer; (2) appropriate particle size and specific surface area, which minimize electrolyte-induced side reactions; and (3) a well-developed hexagonal α-$NaFeO_2$ structure. Spray pyrolysis was shown to be effective for preparing the layered cathode materials $xLi_2MnO_3 \cdot (1-x)LiMO_2$ (M = Ni, Co, Mn). Compared to other processes, spray pyrolysis can be used to prepare composite particles at low calcination temperatures while allowing for the existence of nanosized grains, which can improve electrical performance.

Acknowledgment D. S. J acknowledges the financial support by the "Policy R&D program" funded by the Korea Institute of Ceramic Engineering and Technology, and National Research Foundation of Korea (NRF) funded by the Ministry of Education (NRF-2015R1D1A1A01058334 and GRDC NRF-2015K1A4A3047100), and the Korea Environmental Industry & technology Institute (Grant No. 2014000110003).

References

1) L. Ji, P. Meduri, V. Agubra, X. Xiao and M. Alcoutlabi, *Adv. Energy Mater.*, 6, 1502159–1502232 (2016).
2) A. Andersson, D. Abraham, R. Haasch, S. MacLaren, J. Liu and K. Amine, *J. Electrochem. Soc.*, 149, A1358–A1369 (2002).
3) J.-M. Tarascon and M. Armand, *Nature*, 414, 359–367 (2001).
4) J. Liu, S. Wang, Z. Ding, R. Zhou, Q. Xia, J. Zhang, L. Chen, W. Wei and P. Wang, *ACS Appl. Mater. Interfaces*, 8, 18008–18017 (2016).
5) E. C. Evarts, *Nature*, 526, S93–S95 (2015).
6) B. L. Ellis, K. T. Lee and L. F. Nazar, *Chem. Mater.*, 22, 691–714 (2010).
7) M. M. Thackeray, S.-H. Kang, C. S. Johnson, J. T. Vaughey, R. Benedek and S. Hackney, *J. Mater. Chem.*, 17, 3112–3125 (2007).
8) J.-S. Kim, C. Johnson, J. Vaughey and M. Thackeray, *J. Power Sources*, 153, 258–264 (2006).
9) A. Abouimrane, Y. Cui, Z. Chen, I. Belharouak, H. B. Yahia, H. Wu, R. Assary, L. A. Curtiss and K. Amine, *Nano Energy*, 27, 196–201 (2016).
10) S.-H. Kang, Y. Sun and K. Amine, *Electrochem. Solid-State Lett.*, 6, A183–A186 (2003).
11) M. N. Ates, S. Mukerjee and K. Abraham, *J. Electrochem. Soc.*, 161, A355–A363 (2014).
12) A. R. Armstrong and P. G. Bruce, *Nature*, 381, 499–500 (1996).
13) M. S. Whittingham, *Chem. Rev.*, 104, 4271–4302 (2004).
14) J. Liu, Q. Wang, B. Reeja-Jayan and A. Manthiram, *Electrochem. Commun.*, 12, 750–753 (2010).
15) D. Luo, G. Li, C. Fu, J. Zheng, J. Fan, Q. Li and L. Li, *Adv. Energy Mater.*, 4, 1400062 (2014).
16) J. Liu and A. Manthiram, *J. Mater. Chem.*, 20, 3961–3967 (2010).
17) S.-H. Kang and M. M. Thackeray, *Electrochem. Commun.*, 11, 748–751 (2009).
18) R. Santhanam and B. Rambabu, *J. Power Sources*, 195, 4313–4317 (2010).
19) J.-H. Lim, H. Bang, K.-S. Lee, K. Amine and Y.-K. Sun, *J. Power Sources*, 189, 571–575 (2009).
20) D. Kim, J. Gim, J. Lim, S. Park and J. Kim, *Mater. Res. Bull.*, 45, 252–255 (2010).
21) M. Konarova and I. Taniguchi, *J. Power Sources*, 195, 3661–3667 (2010).

22) S. Park, S.-W. Oh, S. Kang, I. Belharouak, K. Amine and Y.-K. Sun, *Electrochim. Acta*, **52**, 7226–7230 (2007).
23) D. S. Jung, S. B. Park and Y. C. Kang, *Korean J. Chem. Eng.*, **27**, 1621–1645 (2010).
24) J. Y. Seo, K. Lee, S. Y. Lee, S. G. Jeon, J.-G. Na, Y.-K. Oh and S. B. Park, *Bioresour. Technol.*, **152**, 562–566 (2014).
25) J. Y. Seo, H. W. Kang, D. S. Jung, H. M. Lee and S. B. Park, *Mater. Res. Bull.*, **48**, 1484–1489 (2013).
26) C.-C. Wang, K. A. Jarvis, P. J. Ferreira and A. Manthiram, *Chem. Mater.*, **25**, 3267–3275 (2013).
27) J. R. Croy, K. G. Gallagher, M. Balasubramanian, Z. Chen, Y. Ren, D. Kim, S.-H. Kang, D. W. Dees and M. M. Thackeray, *J. Phys. Chem. C*, **117**, 6525–6536 (2013).
28) S.-H. Kang, C. Johnson, J. Vaughey, K. Amine and M. Thackeray, *J. Electrochem. Soc.*, **153**, A1186–A1192 (2006).
29) M. Kotobuki, M. Koishi and Y. Kato, *Ionics*, **19**, 1945–1948 (2013).
30) C. Wan, Y. Nuli, Q. Wu, M. Yan and Z. Jiang, *J. Appl. Electrochem.*, **33**, 107–112 (2003).
31) M. Hou, S. Guo, J. Liu, J. Yang, Y. Wang, C. Wang and Y. Xia, *J. Power Sources*, **287**, 370–376 (2015).
32) C. S. Johnson, N. Li, C. Lefief, J. T. Vaughey and M. M. Thackeray, *Chem. Mater.*, **20**, 6095–6106 (2008).
33) M.-S. Park, J.-W. Lee, W. Choi, D. Im, S.-G. Doo and K.-S. Park, *J. Mater. Chem.*, **20**, 7208–7213 (2010).
34) B. Kang and G. Ceder, *Nature*, **458**, 190–193 (2009).
35) T. Drezen, N.-H. Kwon, P. Bowen, I. Teerlinck, M. Isono and I. Exnar, *J. Power Sources*, **174**, 949–953 (2007).
36) J. H. Kim, S. H. Choi, M. Y. Son, M. H. Kim, J.-K. Lee and Y. C. Kang, *Ceram. Int.*, **39**, 331–336 (2013).
37) Y. Wu and A. Manthiram, *Solid State Ionics*, **180**, 50–56 (2009).